Journal of Translational Medicine

RESEARCH

Open Access

ANGPTL4 mediated mesothelial-mesenchymal transition in pulmonary fibrosis: a potential therapeutic target

Yuechong Xia[1], Fang Zhou[2], Hongyan Hui[2], Liping Dai[3*] and Songyun Ouyang[1*]

Abstract

Background Glycolysis plays a major role in progression of idiopathic pulmonary fibrosis (IPF). Here, we aim to explore the predictive signature based on glycolysis-related genes for predicting the prognosis and identified a potential therapeutic target for IPF.

Methods Gene expression data of bronchoalveolar lavage (BAL) cells and clinical information were downloaded from the Gene Expression Omnibus database. Bioinformatic analysis was then performed to identify differentially expressed genes (DEGs). Lasso multivariate cox analysis and multivariate Cox regression were used to establish a gene signature. The prediction model was evaluated using the time-dependent receiver operating characteristic (ROC) curve and validated using an external independent dataset. The expression of these key genes in cellular level analyzed from Single Cell Expression Atlas. Cell Counting Kit-8 assay, immunofluorescence, wound healing and plasmid transfection were performed.

Results A total of 4 gene (ANGPTL4, ME2, TPBG and IER3), which were associated with the prognosis of IPF patients, were selected to establish our signature. The prediction model was an independent prognostic indicator for IPF patients. ANGPTL4 was significantly upregulated in pleural mesothelial cells (PMCs). In vitro assay showed that ANGPTL4 promoted PMCs proliferation and migration. Knockdown of ANGPTL4 can inhibit mesothelial-mesenchymal transition by suppressed glycolysis-associated gene, such as PGM1, GPI, PGK1, LDHA, ALDOA, ENO1 and TPI1.

Conclusions Our research established a glycolysis-associated gene signature that holds potential to assist clinicians in the personalized management of IPF. Furthermore, we identified that ANGPTL4 mediates mesothelial-mesenchymal transition, suggesting its viability as a therapeutic target for IPF treatment.

Keywords Idiopathic pulmonary fibrosis, Mesothelial-mesenchymal transition, ANGPTL4, Glycolysis

*Correspondence:
Liping Dai
lpdai@zzu.edu.cn
Songyun Ouyang
ouyangsy@163.com
Full list of author information is available at the end of the article

Background

Idiopathic pulmonary fibrosis (IPF) is a chronic interstitial lung disease with a progressive course and characterized by the thickening and scarring of lung tissue [1]. This condition ultimately leads to impaired lung function and a significant decrease in quality of life [1, 2]. Clinically, the median survival time after diagnosis of IPF is 2 to 3 years [1, 3, 4]. Despite the considerable progress in research and treatment of IPF over recent decades, the improvement in the prognosis of IPF patients has been modest at best [5, 6]. Histologically, early stages of IPF are typically characterized by the presence of fibroblastic foci and damage to the lung parenchyma, primarily observed in sub-pleural regions; however, the precise underlying mechanisms remain not fully understood [7, 8].

Pleural mesothelial cells (PMCs) are highly metabolically active cells present as a single-layered epithelium that covers the pleural cavity walls and the visceral layer of the lungs. When exposed to stress or injury, such as inhaled asbestos, PMCs exhibit remarkable plasticity and undergo phenotypic changes, losing their polarity and mesothelial markers. This cellular transformation, known as mesothelial-mesenchymal transition (MMT). Notably, previous studies have provided evidence for the migration of PMCs into the lung parenchyma in pulmonary fibrosis, particularly in sub-pleural areas [9]. Targeting PMCs has demonstrated potential in mitigating the progression of fibrosis, thereby underscoring the critical need to elucidate the role of these cells in the pathogenesis of pulmonary fibrosis [7, 10].

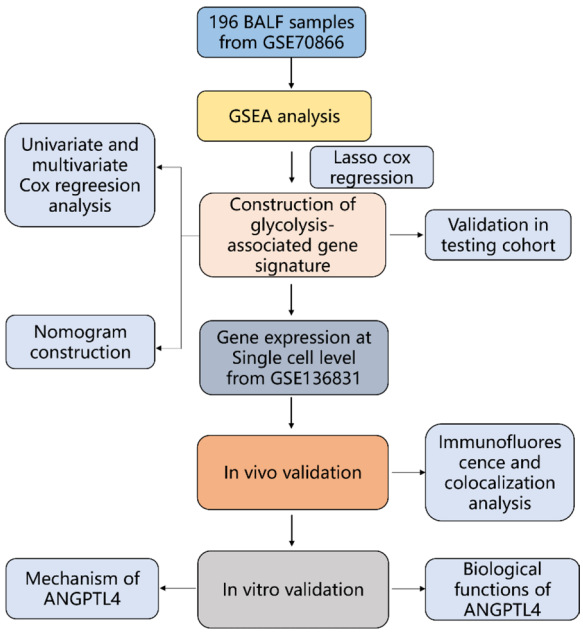

Fig. 1 The flowchart of this study

Angiopoietin-like protein 4 (ANGPTL4) is a multifunctional protein consisting of a helical domain at the N-terminus and a fibrinogen-like domain at the C-terminus. It is expressed in various organs and tissues, including adipose tissue, liver, intestines, and blood [11]. ANGPTL4 plays crucial roles in regulating lipid and glucose metabolism, as well as participating in the transition of macrophage activity and modulating inflammatory responses in different tissues, such as acute pancreatitis and cardiac injury repair [12, 13]. In this study, we conducted a comprehensive analysis of bulk RNA-seq datasets and single-cell sequencing data from IPF patients, revealing the upregulation of ANGPTL4 in IPF. Besides, the role of ANGPTL4 in PMCs was finally verified by cytological experiments. The detailed flowchart was shown in Fig. 1A. These findings indicate that targeting ANGPTL4 could be a new therapeutic approach for treating IPF.

Methods

Publical data acquisition and processing

The gene expression matrix file and associated clinical data for dataset GSE70866 were procured from the Gene Expression Omnibus (GEO) database (https://www.ncbi.nlm.nih.gov/geo/). Samples lacking complete clinical data were excluded from the analysis, yielding a final dataset comprising 20 healthy donors and 62 patients with idiopathic pulmonary fibrosis (IPF) from Freiburg, 50 patients from Siena, and 64 patients from Leuven [14]. Quantile normalization was performed on the dataset utilizing the limma package (version 3.58.1) in R. Furthermore, batch effects were mitigated through the application of the SVA package in R (version 3.50.0) [15]. Platform annotation files were employed to annotate the probes, and for genes represented by multiple probes, the mean gene expression level was computed for subsequent analysis. Differentially expressed genes (DEGs) between IPF patients and healthy donors were identified using the limma package, with a significance threshold set at $p < 0.05$.

The scRNA-seq data from GSE136831 were obtained from the GEO database [16]. Following quality control procedures, a total of 34,464 cells were retained for downstream analyses. The R package "Seurat" (v4.1.1) was utilized for the subsequent data analysis steps [17]. To normalize the scRNA-seq data, we employed the Seurat "NormalizedData" function with default parameters. Highly variable genes were using the Seurat "FindVariableFeatures" function, specifying the parameters "selection.method = vst" and "nfeatures = 2000". The data were then scaled using the Seurat "ScaleData" function. For dimension reduction analysis, the Seurat "RunPCA"

function was applied. To correct for batch effects among all samples, the R package "harmony" (v0.1.1) was utilized by running the "RunHarmony" function. Non-linear dimensional reduction was performed using the Seurat "RunUMAP" function. The expression of classical marker genes for major cell types was assessed.

Gene set enrichment analysis

The complete set of dysregulated genes between idiopathic pulmonary fibrosis (IPF) patients and healthy donors was utilized for gene set enrichment analysis (GSEA). Hallmark gene sets were sourced from the Molecular Signatures Database (MSigDB, www.gsea-msigdb.org/gsea/msigdb), and the Z-scores of these hallmarks were quantified based on transcriptome profiling data.

Construction of risk model and validation

Firstly, Univariate Cox analysis was performed to evaluate the relationship between gene set of glycolysis and the survival time of IPF patients using the survival package (v3.5–8). Genes with $p < 0.001$ were selected for further study. The least absolute shrinkage and selection operator (LASSO) Cox regression was employed using five-fold cross-validation to obtain the most strongly survival-associated genes in the training dataset via glmnet package (v4.1–8). Based on the prognostic model, the risk score of each patient was calculated according to the following formula: risk score = $\beta1 * 1 + \beta2 * 2 + \ldots + \beta n * Xn$ (β, regression coefficient; X, expression of X gene). According to the median of risk scores in the training dataset, Patients in both the training and validation cohorts were divided into high-risk or low-risk groups.

Time-dependent receiver operating characteristic (ROC) curve analysis was used to assess the prognostic performance of the model using the survivalROC package (v1.0.3.1). Additionally, an external validation cohort was used to confirm the predictive value of the prognostic model. To assess the independent predictive value of risk model, univariate and multivariate Cox regression analyses were performed with adjustment for confounding factors, including age, and gender at baseline. Finally, we constructed the nomogram to predict the survival probability of IPF patients. The calibration curves were used to assess the accuracy of this nomogram.

PMCs culture and transfection

The human pleural mesothelial cell line, Met-5A (Cas9x, Suzhou, China), was cultured in a Met-5A cell-specific medium (Cas9x, Suzhou, China). The cells were maintained in a CO2 incubator at 37 °C. Human recombinant TGF-β1 (Peprotech, USA) was dissolved in water to prepare a working solution, and the stock solution was subsequently diluted to a concentration of 10 μg/ml in the culture medium.

When cells were 60–70% confluence, we used Lipofectamine 3000 (Invitrogen, USA) to transfect negative control plasmids (sh-NC) and ANGPTL4-targeted plasmids (sh-ANGPTL4) (GenePharma, China) into cells. 24 h after transfection, the cells were exposed to TGF-β1 24 h. Expression levels of ANGPTL4 were determined by immunoblotting and RT-qPCR.

Animal model and ethics statement

Animal experiments were conducted in strict compliance with the guidelines established by the Ethics Committee of Animal Experiments at The First Affiliated Hospital of Xinxiang Medical University. Twenty male C57BL/6 mice, aged twelve weeks, were randomly divided into two groups. The experimental group (n = 10) received an orotracheal instillation of bleomycin (BLM, Selleck) at a dosage of 5 mg/kg, dissolved in saline, while under anesthesia [18–20]. The control group (n = 10), referred to as the sham group, was administered an equivalent volume of saline only. Twenty-one days after BLM administration, the mice were euthanized for subsequent analysis.

Pathological staining

Pulmonary tissues were fixed in 4% paraformaldehyde and embedded in paraffin. The paraffin blocks were then sectioned at a thickness of 5 μm using a microtome. Sections were stained with Masson's Trichrome and Hematoxylin and Eosin (H&E) [21].

Immunofluorescence and colocalization analysis

Double immunofluorescence co-localization studies were conducted on formalin-fixed, paraffin-embedded (FFPE) mouse lung sections to identify the expression of ANGPTL4 in PMCs. Following deparaffinization, rehydration, and antigen retrieval, non-specific binding was blocked for 1 h at room temperature. The slides were then sequentially incubated with primary antibodies, followed by incubation with horseradish peroxidase (HRP)-conjugated secondary antibodies and subsequent tyramide signal amplification. Nuclei were counterstained with a DAPI-containing anti-fading agent. Images were captured using an SP5 Leica confocal microscope.

Western blot analysis

Protein levels in cells were measured by Western blot analysis. After PMCs were harvested, medium-strength RIPA lysis buffer (Beyotime, Shanghai) was used to fully lyse cells and the protein concentration was determined using the BCA protein assay kit (Beyotime, Shanghai).

Cell lysates were denatured and electrophoresed on SDS-PAGE gel. Separated proteins were electro-transferred to nitrocellulose membranes. The membrane was blocked with 5% milk for 1 h in TBST and incubated with primary antibody against ANGPTL4 (Proteintech, dilution 1:500), CDH1 (Proteintech, dilution 1:2000), FN1 (Abcam, dilution 1:1000) and ACTB (Proteintech, dilution 1:1000) at 4 °C overnight. Secondary antibodies were incubated at room temperature for 1 h. The chemiluminescent images were obtained using the ECL Chemiluminescence Substrate Kit (Servicebio. China).

Cell migration assay

Seed the cells in the 6-well plates and allow them to grow and then were transfected with shRNA 24 h. When cells form a confluent monolayer, we gently scratch the cell layer using a 200ul micropipette tip and remove any detached cells with PBS. The Areas between each edge of the scratch at 0 and 24 h after exposing to TGF-β1 were measured using microscope (Olympus, Japan).

Cell proliferation assay

Following transfection, cells were seeded into 96-well plates at a density of 5000 cells per well. Cell viability was evaluated using the Cell Counting Kit-8 assay (APExBIO, USA), with absorbance readings taken at 450 nm using a microplate reader at 24, 48, and 72 h post-seeding.

RNA extraction and RT-qPCR

Total RNA was isolated from the cells utilizing the GeneJET RNA Extraction Kit (Thermo Fisher Scientific, Waltham, USA) and subsequently reverse transcribed into complementary DNA (cDNA) using the Prime Script RT Reagent Kit (Servicebio, China). Quantitative PCR (qPCR) was performed with the SYBR Green Master Mix Kit (Servicebio, China) on an Applied Biosystems 7500 Real-Time PCR System. The primer sequences are detailed in Additional file 1: Table.S1. The relative mRNA expression levels were quantified employing the $2^{-\Delta\Delta Ct}$ method.

Lactate assay

Lactate levels were quantified using a lactic acid assay kit (Nanjing Jiancheng Bioengineering Institute, Nanjing) in accordance with the manufacturer's instructions. Culture medium (100 μL) was collected 24 h post-exposure to TGF-β1 and transferred to a 5 mL centrifuge tube. Following a 10-min incubation with the working solution and chromogenic agent at 37 °C, 1 mL of stop solution was added to each tube. Absorbance was measured at a wavelength of 530 nm using a microplate reader. The lactate concentration was subsequently normalized to the protein concentration.

Statistical analysis

In this study, statistical analyses were conducted using R software (v4.0.5) and GraphPad Prism (v8.0). Results are expressed as the mean ± standard error of the mean (SEM). Normality and homogeneity of variance tests were performed on the measurement data for each group. One-way ANOVA was applied to data that met the assumptions of normal distribution and homogeneity of variance. If the variable did not follow a normal distribution, the Wilcoxon or the Kruskal–Wallis test was performed. Survival times were estimated using the Kaplan–Meier (KM) method, and comparisons were conducted with the log-rank test. To control for potential confounders, multivariate Cox regression models were utilized. A p-value of less than 0.05 was considered statistically significant ($^{*}p < 0.05$, $^{**}p < 0.01$, $^{***}p < 0.001$, $^{****}p < 0.0001$).

Results

The glycolytic pathway is activated in IPF

After processing the datasets, "limma" package was used to find different expression genes (DEG) between IPF and health controls (Fig. 2A). Then all genes were used to conduct to GSEA. We found that many pathways were activated in IPF, such as ANGIOGENESIS, EPITHELIAL MESENCHYMAL TRANSITION, MTORC1_SIGNALING and GLYCOLYSIS (Fig. 2B).

Construction of prognostic risk model

As the bioinformatic analysis above. We used the gene set of glycolysis to construct a prognostic risk model. The individuals from Freiburg and Siena were selected as the training set (n = 112) and the patients from Leuven (n = 64) were as the external testing set. First, a univariate Cox regression analysis was performed to consider the association between glycolysis-related gene expression

(See figure on next page.)

Fig. 2 Construction of the glycolysis-associated-gene risk score model. Volcano diagram of the differential expression RNAs between IPF and healthy donor (**A**). GSEA enrichment analyses between IPF and healthy donor (**B**). LASSO regression coefficients under diverse log λ values (**C**). Partial likelihood deviance under diverse log λ values for LASSO (**D**). Forest plot showing the association between the expression level of 4 selected genes and the survival times of patients (**E**). The expression level of 4 selected genes between IPF and healthy donor (**F**). $^{*}P < 0.05$; $^{**}P < 0.01$; $^{***}P < 0.001$

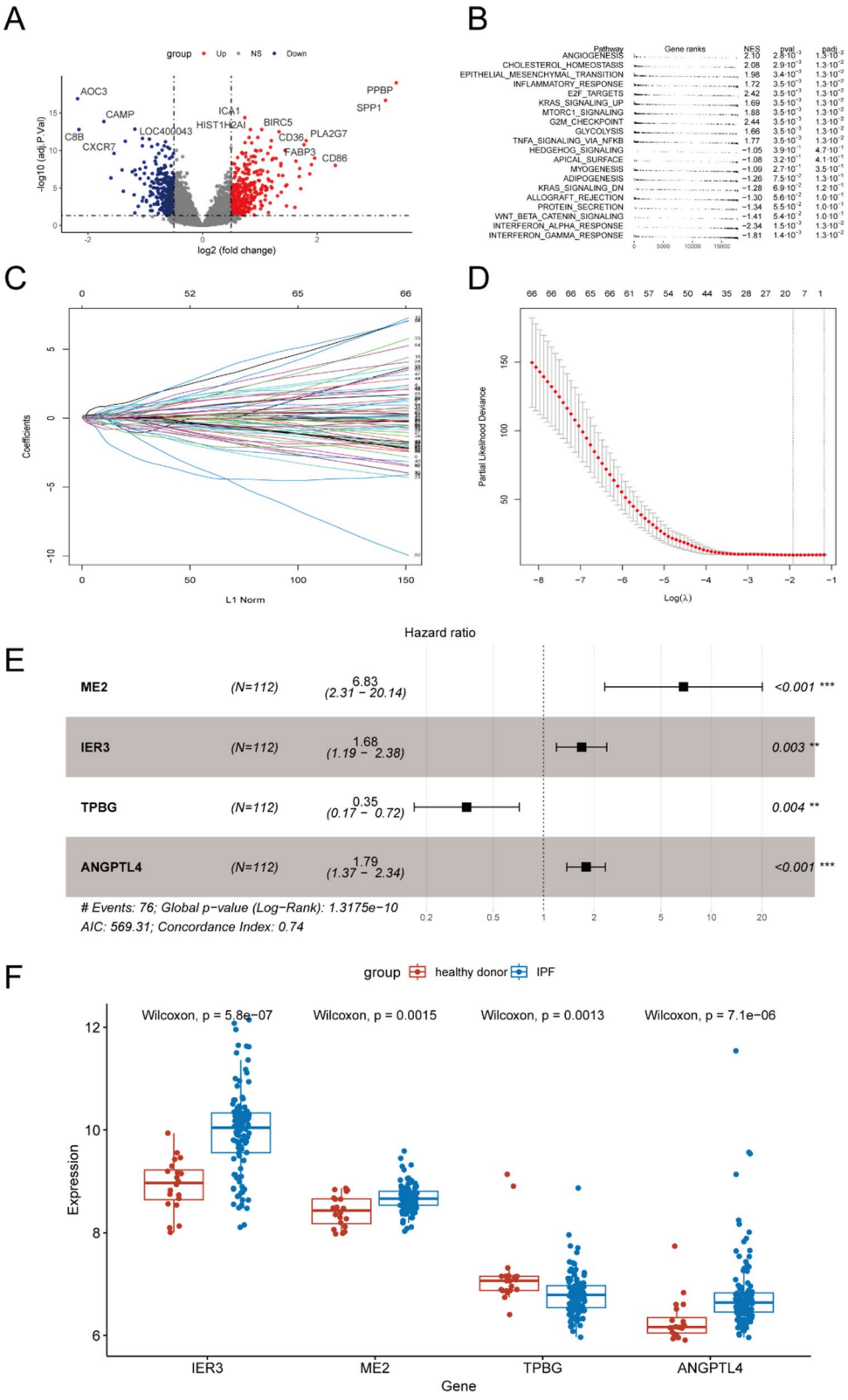

Fig. 2 (See legend on previous page.)

level and IPF survival. Genes with p-value < 0.1 in univariate Cox analysis (Additional file 1: Table.S2) were inputted into LASSO Cox regression (Fig. 2C). Then, 14 genes (Additional file 1: Table.S3) were selected to construct a prognostic model using multivariate Cox regression (Fig. 2D). TPBG, IER3, ME2 and ANGPTL4 were associated with prognosis in multivariate Cox regression and were finally used to construct risk score model (Fig. 2E). Notice that genes ANGPTL4, IER3 and ME2 were highly expressed in patients with IPF, while the TPBG was lowly expressed in IPF (Fig. 2F). The risk score of each patient was calculated using the formula: risk score = (1.921 * expression of ME2) + (0.521 * expression of IER3) + (− 1.057* expression of TPBG) + (0.584 * expression of ANGPTL4).

Four glycolysis-associated gene signature serves as a risk factor for patients with IPF

In the training set, the cohort of 112 patients was stratified into high-risk and low-risk groups according to the median risk scores (Fig. 3A, B). Kaplan–Meier (K-M) analysis demonstrated that the high-risk group exhibited significantly poorer clinical outcomes compared to the low-risk group (P < 0.001, Fig. 3C). Additionally, both univariate and multivariate Cox proportional hazards analyses identified the five-gene signature as an independent prognostic factor (Fig. 3D, E). The area under the receiver operating characteristic curve (AUC) analysis further confirmed the model's robust predictive capability for overall survival in idiopathic pulmonary fibrosis (IPF), with AUC values of 0.803, 0.77, and 0.716 for 1-year, 2-year, and 3-year survival, respectively (Fig. 3F). Finally, we developed a nomogram for clinical application based on the four-gene signature (Fig. 4A). Subsequently, a calibration curve was generated to assess the predictive accuracy of the nomogram (Fig. 4B). The calibration chart demonstrated that the predicted 1-, 3-, and 5-year survival probabilities were in close concordance with the observed outcomes.

In the external test set, the 64 patients were stratified into high and low-risk groups based on the median scores derived from the training data (Fig. 5A, B). Kaplan–Meier (K-M) analysis demonstrated that the high-risk group exhibited significantly poorer clinical outcomes compared to the low-risk group (P = 0.03, Fig. 5C). Additionally, both univariate and multivariate Cox proportional hazards analyses identified the five-gene signature as an independent risk factor (Fig. 5D, E). The AUC analysis confirmed the robust predictive capability of the model for overall survival in idiopathic pulmonary fibrosis (IPF), with AUC values of 0.696, 0.705, and 0.688 for 1-, 2-, and 3-year survival, respectively (Fig. 5F).

ANGPTL4 is highly expressed in mesothelial cells

Next, the single cell sequence dataset of GSE136831 was used to explored the expression of four genes at single cell level. According to the classical gene markers of lung cells, three major cell types were identified in lung tissue, such as epithelial cell, immune cells and stromal cells (Additional file 1: Fig. S1). We then performed subcluster analysis to illustrate the gene expression of each cell type. First, Epithelial cells were re-clustered into four clusters and the major lung epithelial cell types were readily identified with classical cell markers (Fig. 6A, B). Immune cells were re-clustered into ten clusters and the major lung immune cell types were readily identified with classical cell markers (Fig. 6C, D). Stromal cells were re-clustered into seven clusters and the major lung stromal cell types were readily identified with classical cell markers (Fig. 6E, F). The dot plot showed ANGPTL4, IER3 and TPBG were mainly expressed in epithelial and stromal cells. ME2 were mainly expressed in immune cell (Fig. 6G–I). We mainly focused on stromal cells for further analysis because of its key roles in IPF. We revealed that ANGPTL4 is significantly higher expressed in mesothelial cells of IPF when compared with healthy control and COPD (Fig. 6J). MMT is activated in PMCs of IPF when compared with healthy control (Fig. 6K).

ANGPTL4 is upregulated in MMT

Previous studies had reported that mesothelial cell traffic to parenchymal region of lung by MMT [7]. The presence of PMCs in vivo was further substantiated by multiplex immunofluorescence staining. The lung tissue in the BLM group displayed structural disorganization and significant collagen deposition, as evidenced by H&E and Masson staining, confirming the success of the modeling (Additional file 1: Fig. S2). The results of colocalization analysis showed that PMCs traffic to parenchymal region when mouse exposing to BLM. ANGPTL4 and Calretinin can colocalized in some cells, which demonstrated that PMCs highly expressed ANGPTL4 in MMT (Fig. 7A).

In vitro, when Met-5A exposed to 10 ng/ml TGF-β1 for 24 h, FN was upregulated and CDH1 was downregulated in RNA and protein levels (Fig. 7B–D). The results indicate that TGF-β1 can induce MMT in Met-5A. We next evaluated the expression of ANGPTL4 in MMT. The results showed that ANGPTL4 was upregulated in MMT (Fig. 7E, F).

Knockdown of ANGPTL4 suppress MMT in PMCs

We transfected sh-ANGPTL4 in MET-5A to determine whether knockdown of ANGPTL4 can inhibit MMT. First, 24 h post-transfection with sh-ANGPTL4 plasmid, the cells were exposed to TGF-β1 for 24 h. The transfection efficiency was assessed with RT-qPCR

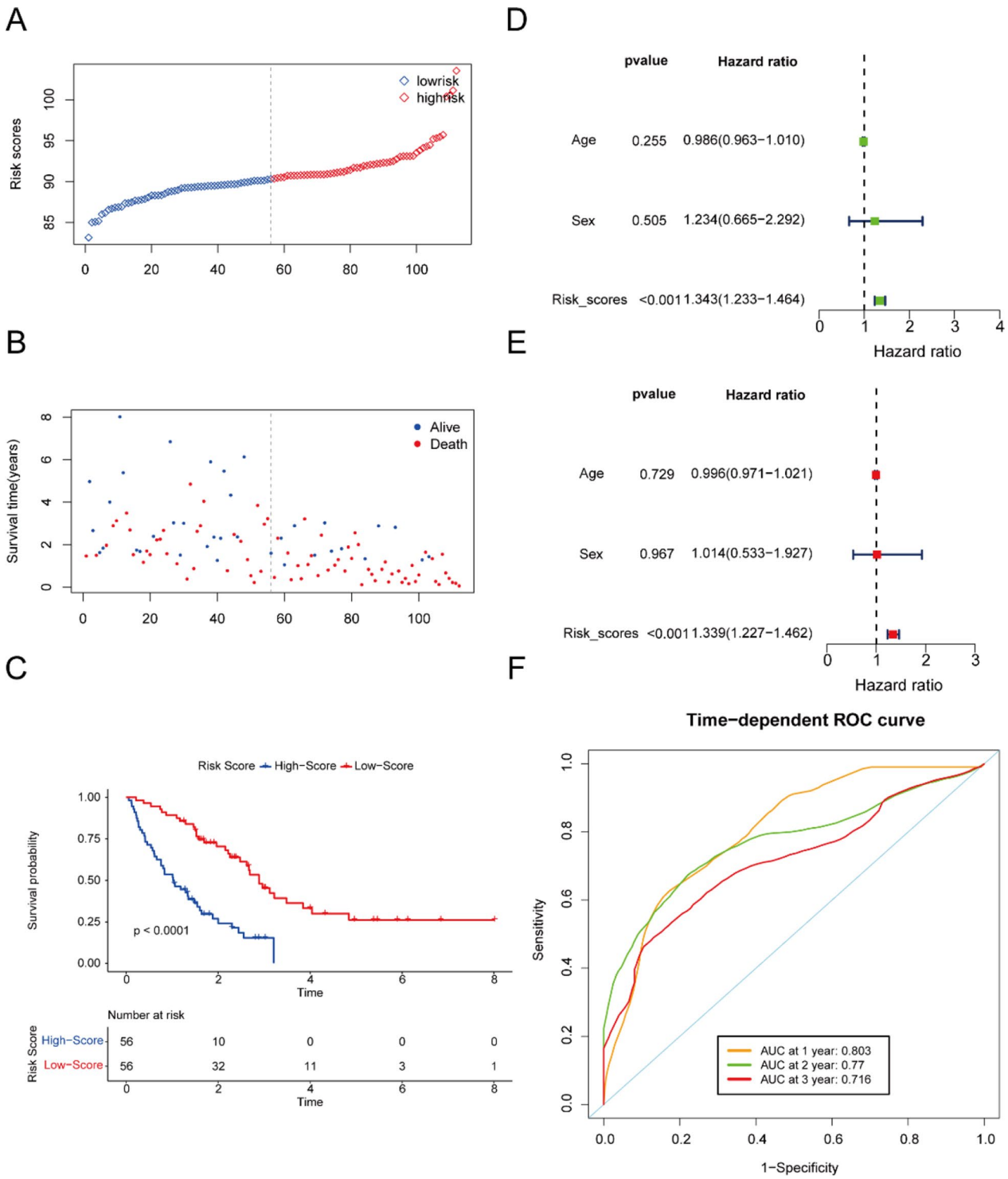

Fig. 3 Prognostic analysis of the risk score formula in the training set. Distribution of risk score for the training set (**A**). Patterns of the survival time and survival status between the high-risk and low-risk groups for training set (**B**). Kaplan–Meier survival curve of the patients in the high-risk and low-risk groups for survival in the training set (**C**). Univariate (**D**) and multivariate (**E**) Cox regression analysis for the risk score and other clinical characteristics for training set. Time-related ROC analysis proved the prognostic performance of the risk score in the training set (**F**)

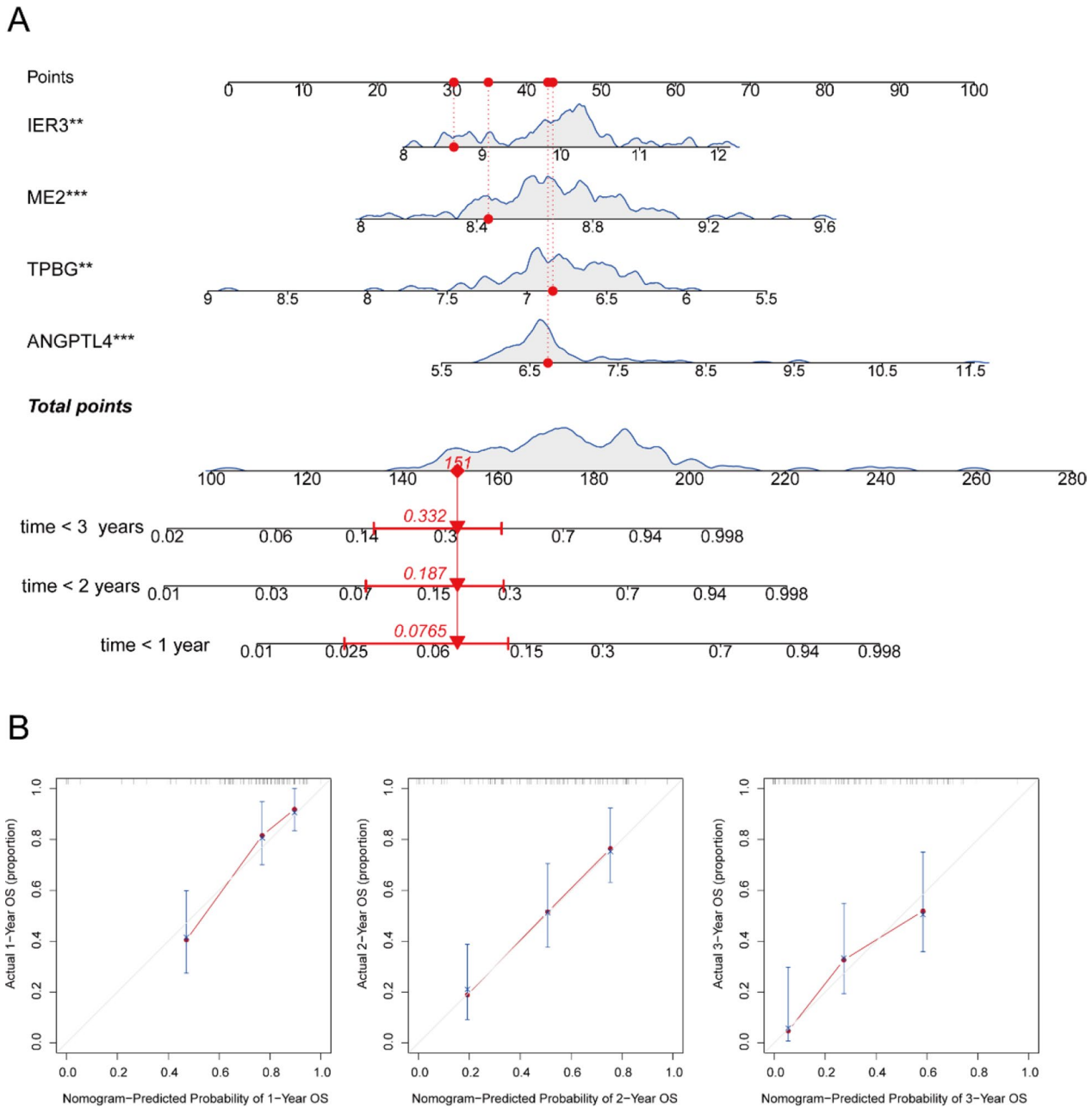

Fig. 4 Construction of the nomogram predicting the survival possibilities at 1-, 2-, and 3-years (**A**). Correction curve showing the consistency between predicted survival possibilities and the observed survival rate (**B**)

and Western blot (Fig. 8A–C). The results showed that ANGPTL4 was suppressed more efficient when cells were transfected with sh-ANGPTL4 #2. Second, we evaluated the expression of FN and E-cadherin when knockdown ANGPTL4. The results showed that knockdown of ANGPTL4 inhibited MMT (Fig. 8D–F).

ANGPTL4 promote proliferation and migration of PMCs

Wound healing and CCK8 assays were performed to explore the role of ANGPTL4 in migration and proliferation of PMCs. Knockdown of ANGPTL4 by shRNA in MET-5A reduced wound healing after 24 h, indicating ANGPTL4 suppressed the migration of MET-5A

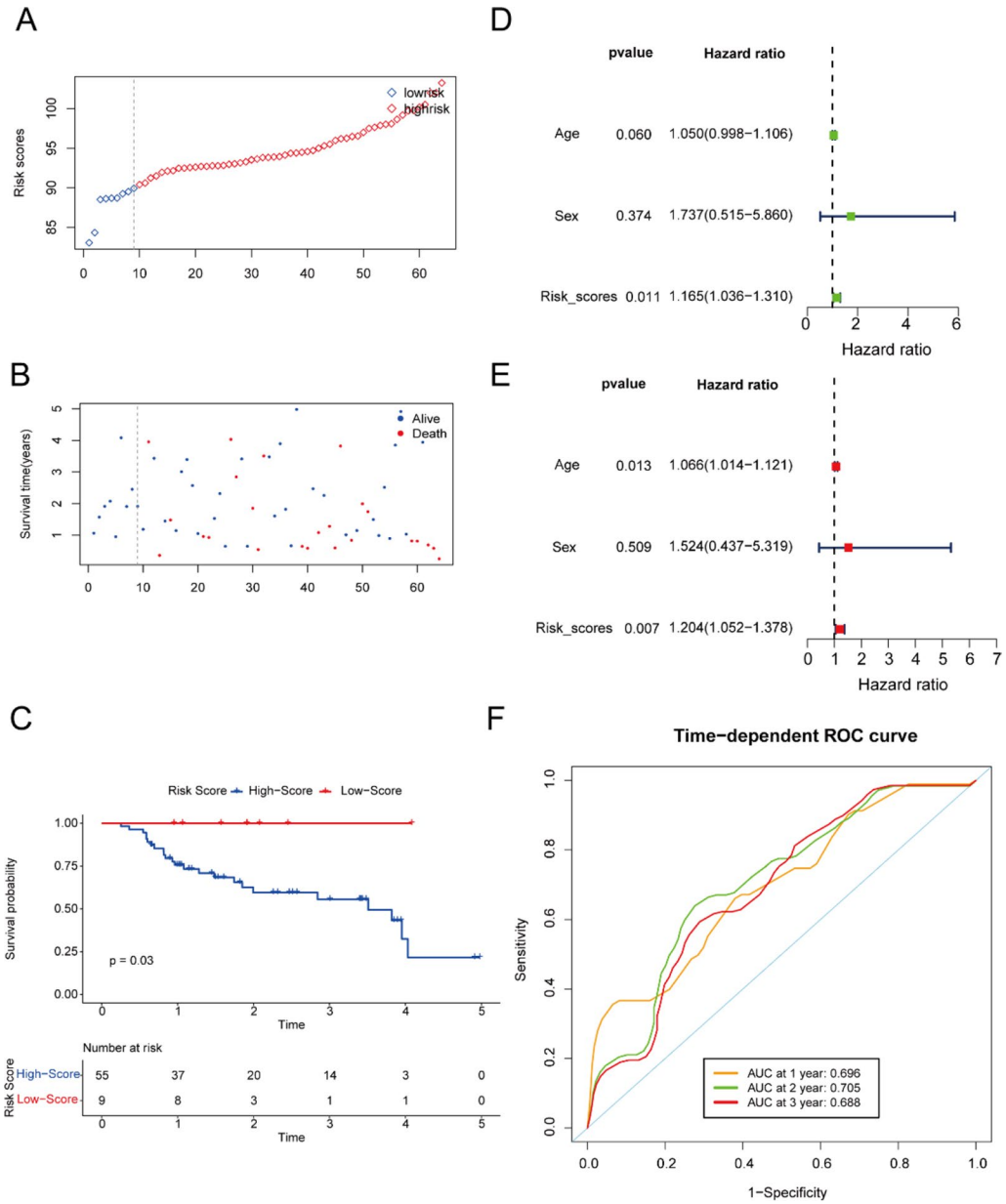

Fig. 5 Prognostic analysis of the risk score formula in the testing set. Distribution of risk score for the testing set (**A**). Patterns of the survival time and survival status between the high-risk and low-risk groups for testing set (**B**). Kaplan–Meier survival curve of the patients in the high-risk and low-risk groups for survival in the testing set (**C**). Univariate (**D**) and multivariate (**E**) Cox regression analysis for the risk score and other clinical characteristics for testing set. Time-related ROC analysis proved the prognostic performance of the risk score in the testing set (**F**)

(See figure on next page.)

Fig. 6 The mRNA expression of 4 selected genes in IPF at single cell level. UMAP plots showing the distribution of classical subpopulations of epithelial cells (**A**), immune cell (**C**) and stromal cells (**E**). Dot plots showing the expression of marker genes corresponding to epithelial cell subpopulations (**B**), immune cell subpopulations (**D**) and stromal cell subpopulations (**E**). The mRNA expression of 4 selected genes in epithelial cell subpopulations (**G**), immune cell subpopulations (**H**) and stromal cell subpopulations (**I**). The expression of ANGPTL4 in PMCs (**J**). MMT is activated in PMCs of IPF when compared with healthy control (**K**)

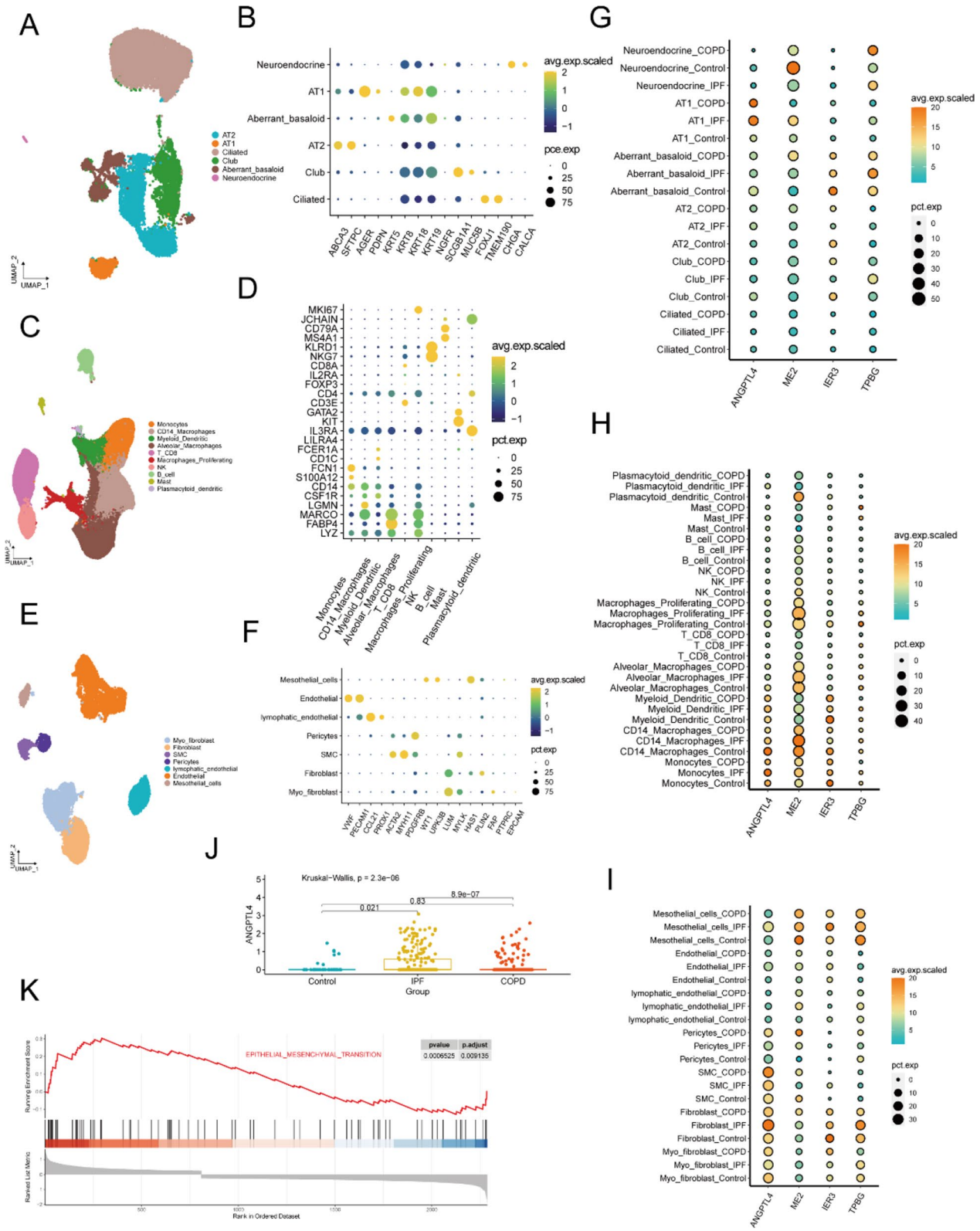

Fig. 6 (See legend on previous page.)

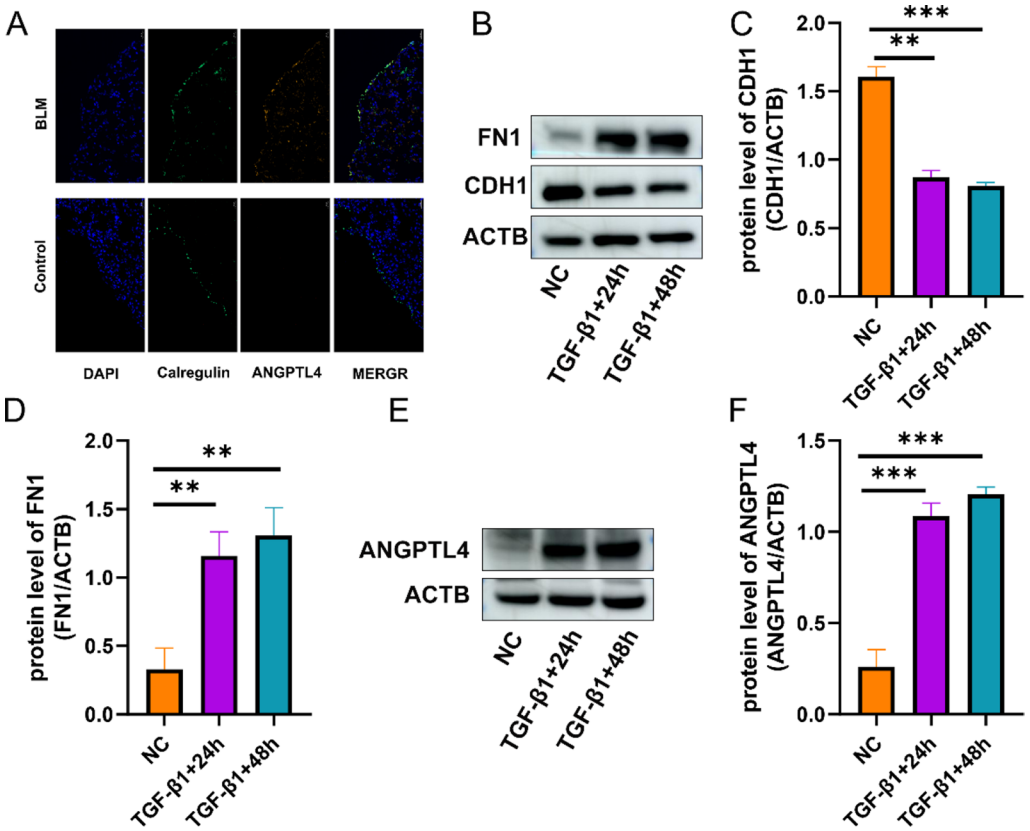

Fig.7 ANGPTL4 is upregulated in MMT. PMCs migrate to the parenchymal region in response to exposure to bleomycin (BLM) in mice, exhibiting relatively high expression levels of ANGPTL4 (**A**). TGF-β1 induce MMT in Met-5A (**B**–**D**). ANGPTL4 was upregulated in MMT (**E**, **F**). *P < 0.5; **P < 0.01; ***P < 0.001

(Fig. 8G, H). Moreover, ANGPTL4 knockdown significantly inhibited proliferation of MET-5A (Fig. 8I). These observations, taken together, suggested that ANGPTL4 is crucial in modulating proliferation and migration of PMCs.

ANGPTL4 promote MMT by activating glycolysis

Previous study has revealed ANGPTL4 inhibited glycolysis in endothelial cells [11]. Figure 9A illustrates the significant rate-limiting genes (depicted in green) involved in glycolysis. RT-qPCR was performed to validated the expression of those glycolysis-associated genes in PMCs with ANGPTL4 knockdown. The results showed that knockdown of ANGPTL4 suppressed those glycolysis-associated genes such as PGM1, GPI, PGK1, LDHA, ALDOA, ENO1 and TPI1 (Fig. 9B). Lactate assay showed that knockdown of ANGPTL4 can reduce the lactate levels in media from cultured cells (Fig. 9C). 2-DG is a glycolysis inhibiter and is used as a positive control. 2-DG inhibited the MMT in TGF-β1-induced cells, which indicated glycolysis is a driver of MMT (Additional file 1: Fig. S3). Collectively, these data indicated that ANGPTL4 promote MMT by activating glycolysis and promote fibrosis in subpleural (Fig. 9D).

Discussion

In this study, combined with follow-up data, a four-gene signature predictive model was constructed based on BALF transcriptomic data from IPF. We revealed that the expression of ANGPTL4 was associated with prognostic of IPF patients. The expression of ANGPTL4 was mainly in PMC and significantly upregulated in IPF patients. Some wet experiments were carried out to validated the above results and the mechanism of ANGPTL4 in MMT. The results showed targeting ANGPTL4 inhibited MMT by downregulated glycolysis process.

Although two antifibrotics have been approved in the past decade, there are no curative therapies except lung transplant. Clear criteria for determining the timing of antifibrotic treatments are not currently available [22]. Clinically, delays are not uncommon [22]. IPF is an invariably progressive disease and it is of significant implication

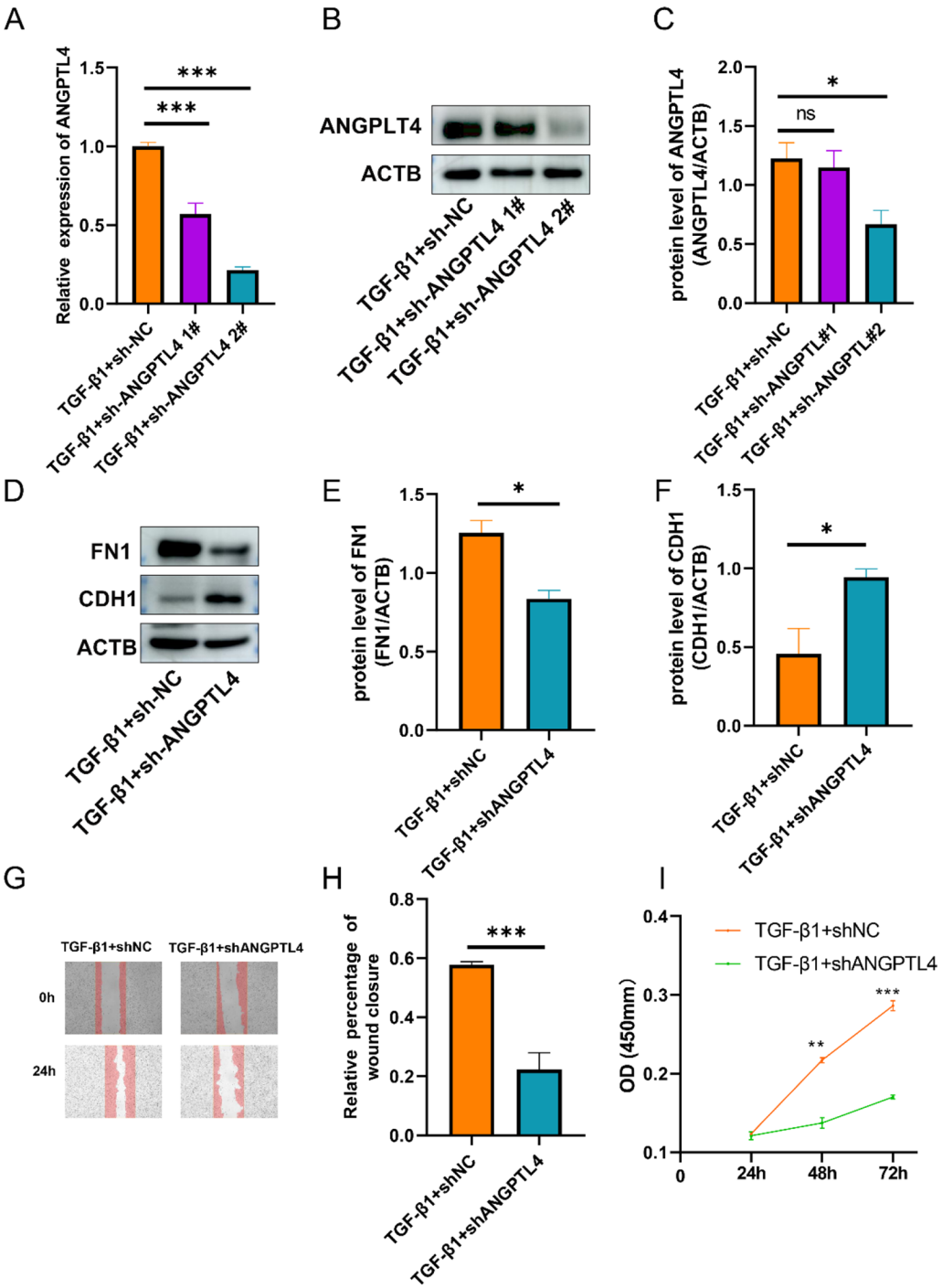

Fig. 8 Knockdown of ANGPTL4 suppress MMT in PMCs. The mRNA expression and protein level of ANGPTL4 in MMT after transferring with sh-ANGPTL4 was determined by qRT-PCR and WB (**A**–**C**). The protein level of FN1 and CDH1 in MMT after transferring with sh-ANGPTL4 was determined by WB (**D**–**F**). Cell migration was detected by wound healing (**G**, **H**). The proliferation abilities of PMCs were detected by CCK-8 (**I**). *P < 0.5; **P < 0.01; ***P < 0.001

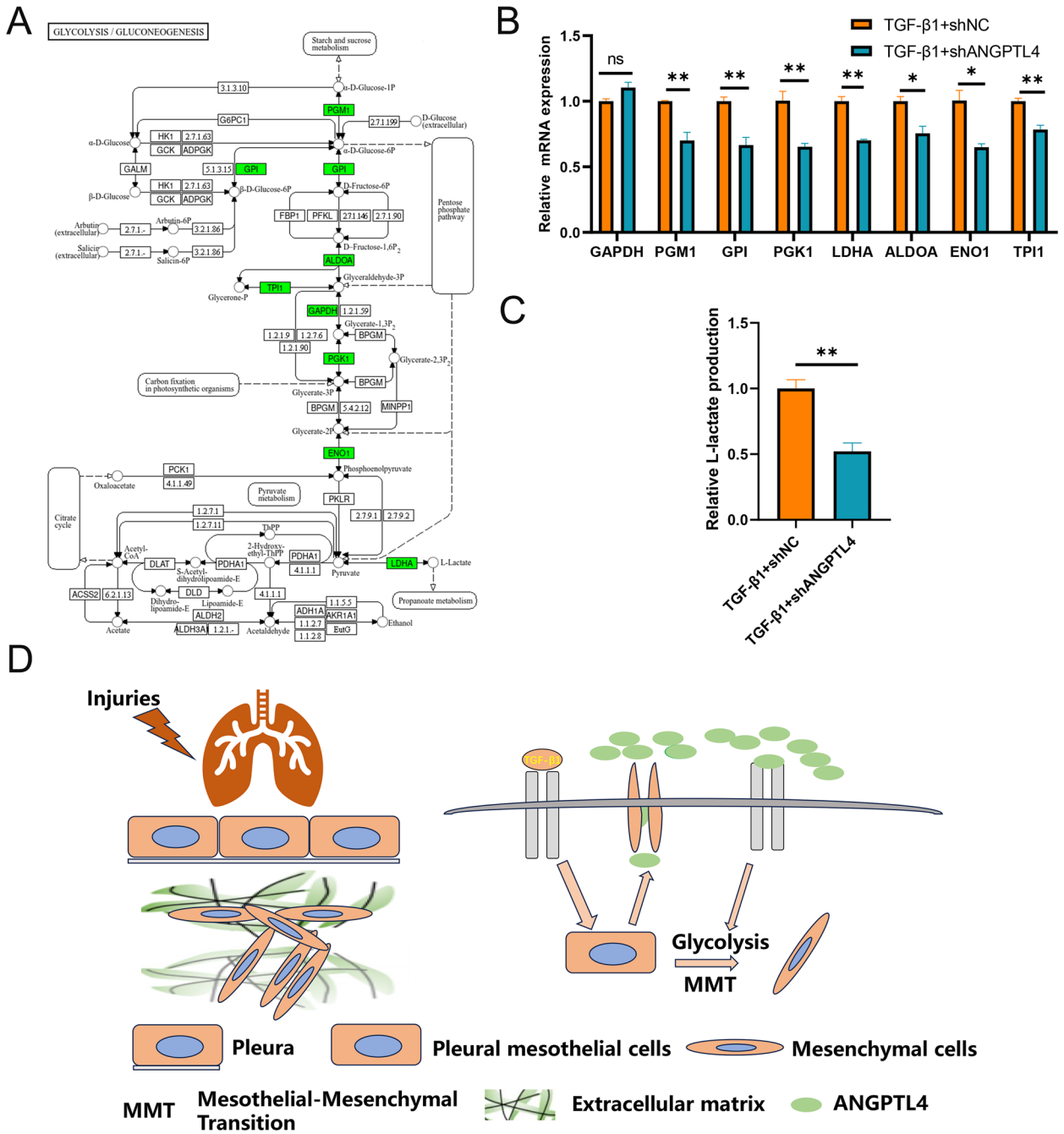

Fig. 9 ANGPTL4 promote MMT by activating glycolysis. Glycolysis/gluconeogenesis pathway and green represents important rate-limiting genes in pathway (**A**). The mRNA expression of glycolysis genes was validated by qRT-PCR (**B**). Cell culture supernatant L-lactate level after knockdown of ANGPTL4 (**C**). Mechanistic diagram illustrating the role of ANGPTL4 in pulmonary fibrosis (**D**)

to predict prognosis of IPF patients in management. In our study, we constructed a glycolysis-associated gene signature, which showed a moderate performance for predicting one-year, two-year, and three-year survival rates in the training and testing datasets. Our gene signature can identify patients at risk of severe disease and remind clinicians to initiate treatment earlier.

Our study revealed that MMT was significantly activated in IPF in PMCs. IPF predominantly occur in subpleural and the mechanism is still poorly understood. Fibroblasts are generally considered to be the key effector

cells in pulmonary fibrosis [23]. Fibroblasts can turn into myofibroblasts when exposed to cytokines, such as TGF-β1, and get stronger extracellular matrix secretion ability, anti-apoptosis, active proliferation, enhanced invasion [23]. Many cell types can turn into myofibroblasts exclude fibroblast, such as alveolar epithelial cells, vascular endothelial cells, macrophages [24, 25]. Previous studies has reported that PMCs exposed to TGF-β1 lead to pleural fibrosis, which indicated the PMCs have full potential in organ fibrosis [26]. Interestingly, when mouse exposed to inhaled TGF-β1, PMCs could traffic into lung parenchyma and subpleural fibrosis is occurred [9]. PMCs were found in BLAF of pulmonary fibrosis mouse model. The numbers of PMCs in parenchyma were positive correlation with Ashcroft score in IPF patients [9]. A study found that epithelial cells along the honeycombing and fibroblastic foci highly expressed LRRN4, which is considered a marker of PMCs [27]. Overall, PMCs in parenchyma might be a predictive factor for the severity of fibrosis and preventing PMCs to traffic into parenchyma maybe a novel therapeutic strategies for the treatment of pulmonary fibrosis.

Excessive accumulation and deposition of extracellular matrix components is the most important features of IPF. More and more studies have shown that metabolic reprogramming plays a key role in the occurrence and development of pulmonary fibrosis, and targeting pulmonary myoblast metabolism can alleviate pulmonary fibrosis in experimental mice [28–31]. In this study, when exposing to 2-DG, MMT was significantly inhibited. The results indicated that glycolysis plays key roles in MMT. These findings suggest that rapidly proliferating and metabolically active myofibroblasts in pulmonary fibrotic tissues may undergo aerobic glycolysis (Warburg phenomenon) like tumor cells [30]. Previous studies have shown that lactate levels in TGF-β1-induced differentiated fibroblasts are significantly higher than in untreated controls, and lactate levels are also significantly higher in IPF lung tissue or mouse pulmonary fibrosis models [28]. Lactic acid level significantly increased during MMT. Knockdown of ANGPTL4 decreased lactic acid level by suppressing glycolysis. Lactic acid is not only the end products of glycolysis, it also can mediate epigenetic modification by protein lactylation. Previous studies have revealed that lactate promote macrophage profibrotic activity through lactate-induced histone lactylation [32]. The lactate from PMCs may mediate the interaction between PMCs and macrophage. Knockdown of ANGPTL4 in PMCs may suppressed macrophage profibrotic activity, which needed further validation.

In this study, ANGPTL4 was selected as a target gene that has a gradual increase according to the survival analysis and scRNA analysis. Its expression was significantly elevated in PMCs and negatively associated with survival time of IPF patients. ANGPTL4 has multifaceted functions and its physiological roles may be largely dependent on the pathological conditions. One study revealed that ANGPTL4 as a downstream of mTOR pathway and promote epithelial-mesenchymal transition in A549 (lung epithelial cells) [33]. Another study demonstrated that ANGPTL4 was predominantly expressed in the activated fibroblasts and myofibroblasts, knockdown of ANGPTL4 suppressed the gene expression of fibrosis-related markers [34]. Those studies demonstrate that ANGPTL4 is critical for the progression of IPF, however, the underlying mechanism of ANGPTL4 was not illustrated clearly. In this study, we demonstrated that ANGPTL4 promote MMT by upregulating expression of the glycolysis-associated genes.

Previous studies have shown that ANGPTL4 is upregulated in influenza pneumonia and increases pulmonary tissue leakiness. The ANGPTL4 monoclonal antibody can reduce lung damage and help patients recover faster, suggesting it may be a future therapeutic strategy for treating influenza pneumonia [35]. In our study, we found that ANGPTL4 mediates MMT, and knocking down ANGPTL4 can suppress this process. The ANGPTL4 monoclonal antibody may also be a potential treatment for pulmonary fibrosis. However, as a biologic agent, it may induce B cell activation, leading to the generation of anti-drug antibodies (ADAs) due to immunogenicity, which can result in resistance to these therapeutics [36]. To reduce the immunogenicity of biologics and prevent resistance, strategies could include altering chemical modifications, improving purification methods, or changing the route and dosage of administration [36, 37].

There are some deficiencies in our study. Firstly, we could not validate the co-localization of ANGPTL4 with calretinin in IPF lung tissues due to challenges in obtaining these samples. Furthermore, researchers have reported that tail vein injection of BLM creates a pulmonary fibrosis model that more accurately represents IPF compared to intratracheal or intraperitoneal administration [20]. However, we did not investigate the expression of ANGPTL4 in the mouse model induced by tail vein injection of BLM. Thirdly, we did not carry out studies to demonstrate whether genetic knockdown of ANGPTL4 can ameliorate subpleural fibrosis in mouse exposing to BLM. Fourthly, ANGPTL4 as a secretory protein, we did not demonstrate whether it can act on neighboring cells, especially interaction with macrophages. Those questions are of great interest for our future studies.

Conclusion

A gene signature associated with glycolysis, comprising ANGPTL4, IER3, ME2, and TPBG, was developed. This signature demonstrated independent prognostic predictive capability and exhibited superior predictive performance. It may be helpful to assist clinicians in making treatment decisions in the individualized management of IPF. Furthermore, ANGPTL4 is markedly upregulated in PMCs and facilitates mesothelial-mesenchymal transition in the context of pulmonary fibrosis. Consequently, ANGPTL4 may represent a promising therapeutic target for IPF.

Abbreviations

IPF	Idiopathic pulmonary fibrosis
BALF	Bronchoalveolar lavage fluid
DEGs	Differentially expressed genes
ANGPTL4	Angiopoietin-like protein 4
ME2	Malic enzyme 2
TPBG	Trophoblast glycoprotein
IER3	Immediate early response 3
PMCs	Pleural mesothelial cells
PGM1	Phosphoglucomutase 1
GPI	Glucose-6-phosphate isomerase
PGK1	Phosphoglycerate kinase 1
LDHA	Lactate dehydrogenase A
ENO1	Enolase 1
ALDOA	Aldolase, fructose-bisphosphate A
TPI1	Triosephosphate isomerase 1
GSEA	Gene set enrichment analysis
LASSO	Least absolute shrinkage and selection operator
BLM	Bleomycin
ACTB	Actin beta
FN1	Fibronectin 1
CDH1	Cadherin 1
HE	Hematoxylin and eosin
MT	Masson's trichrome stain

Supplementary Information

The online version contains supplementary material available at https://doi.org/10.1186/s12967-024-05869-2.

Additional file 1.

Additional file 2.

Additional file 3.

Additional file 4.

Additional file 5.

Additional file 6.

Acknowledgements

We thank the GEO database for sharing the data.

Author contributions

SO and LD conceived the study and designed the experiments. YX performed the bioinformatics analyses, data analysis and drafted the article. YX was responsible for conducting the experimental validation. FZ and HH performed the mouse experiments. All authors contributed to revising the manuscript critically for important intellectual content and have given final approval for the version to be published.

Funding

This research was funded by National Natural Science Foundation of China (No. U1804195).

Data availability

The datasets used and analyzed in this study are available from the Gene Expression Omnibus database (https://www.ncbi.nlm.nih.gov/geo/).

Declarations

Ethics approval and consent to participate

The animal study was reviewed and approved by the Ethics Committee of the First Affiliated Hospital of Xinxiang Medical University.

Consent for publication

Not applicable.

Competing interests

The authors declare no competing interests.

Author details

[1]Department of Respiratory and Critical Care Medicine, the First Affiliated Hospital of Zhengzhou University, Zhengzhou 450052, China. [2]Department of Clinical Pharmacy, The First Affiliated Hospital of Xinxiang Medical University, Weihui, China. [3]Henan Institute of Medical and Pharmaceutical Sciences & Henan Key Medical Laboratory of Tumor Molecular Biomarkers, Zhengzhou University, Zhengzhou 450052, China.

Received: 9 August 2024 Accepted: 9 November 2024
Published online: 20 December 2024

References

1. Richeldi L, Collard HR, Jones MG. Idiopathic pulmonary fibrosis. Lancet. 2017;389(10082):1941–52.
2. Martinez FJ, Collard HR, Pardo A, Raghu G, Richeldi L, Selman M, et al. Idiopathic pulmonary fibrosis. Nat Rev Dis Primers. 2017;3:170–4.
3. Frankel SK, Schwarz MI. Update in idiopathic pulmonary fibrosis. Curr Opin Pulm Med. 2009;15(5):463–9.
4. Kim HJ, Perlman D, Tomic R. Natural history of idiopathic pulmonary fibrosis. Respir Med. 2015;109(6):661–70.
5. Cerri S, Monari M, Guerrieri A, Donatelli P, Bassi I, Garuti M, et al. Real-life comparison of pirfenidone and nintedanib in patients with idiopathic pulmonary fibrosis: a 24-month assessment. Respir Med. 2019;159:105803.
6. Mei Q, Liu Z, Zuo H, Yang Z, Qu J. Idiopathic pulmonary fibrosis: an update on pathogenesis. Front Pharmacol. 2021;12:797292.
7. Zhou LL, Cheng PP, He XL, Liang LM, Wang M, Lu YZ, et al. Pleural mesothelial cell migration into lung parenchyma by calpain contributes to idiopathic pulmonary fibrosis. J Cell Physiol. 2022;237(1):566–79.
8. Raghu G, Collard HR, Egan JJ, Martinez FJ, Behr J, Brown KK, et al. An official ATS/ERS/JRS/ALAT statement: idiopathic pulmonary fibrosis: evidence-based guidelines for diagnosis and management. Am J Respir Crit Care Med. 2011;183(6):788–824.
9. Mubarak KK, Montes-Worboys A, Regev D, Nasreen N, Mohammed KA, Faruqi I, et al. Parenchymal trafficking of pleural mesothelial cells in idiopathic pulmonary fibrosis. Eur Respir J. 2012;39(1):133–40.
10. Zhang Q, Ye H, Xiang F, Song LJ, Zhou LL, Cai PC, et al. miR-18a-5p inhibits sub-pleural pulmonary fibrosis by targeting TGF-beta receptor II. Mol Ther. 2017;25(3):728–38.
11. Chaube B, Citrin KM, Sahraei M, Singh AK, de Urturi DS, Ding W, et al. Suppression of angiopoietin-like 4 reprograms endothelial cell metabolism and inhibits angiogenesis. Nat Commun. 2023;14(1):8251.
12. Jung KH, Son MK, Yan HH, Fang Z, Kim J, Kim SJ, et al. ANGPTL4 exacerbates pancreatitis by augmenting acinar cell injury through upregulation of C5a. EMBO Mol Med. 2020;12(8):e11222.
13. Cho DI, Kang H-J, Jeon JH, Eom GH, Cho HH, Kim MR, et al. Antiinflammatory activity of ANGPTL4 facilitates macrophage polarization to induce cardiac repair. JCI Insight. 2019. https://doi.org/10.1172/jci.insight.125437.

14. Prasse A, Binder H, Schupp JC, Kayser G, Bargagli E, Jaeger B, et al. BAL cell gene expression is indicative of outcome and airway basal cell involvement in idiopathic pulmonary fibrosis. Am J Respir Crit Care Med. 2019;199(5):622–30.
15. Leek JT, Johnson WE, Parker HS, Jaffe AE, Storey JD. The sva package for removing batch effects and other unwanted variation in high-throughput experiments. Bioinformatics. 2012;28(6):882–3.
16. Single-cell RNA-seq reveals ectopic and aberrant lung-resident cell populations in idiopathic pulmonary fibrosis.
17. Stuart T, Butler A, Hoffman P, Hafemeister C, Papalexi E, Mauck WM 3rd, et al. Comprehensive integration of single-cell data. Cell. 2019;177(7):1888-902.e21.
18. Yan P, Yang K, Xu M, Zhu M, Duan Y, Li W, et al. CCT6A alleviates pulmonary fibrosis by inhibiting HIF-1α-mediated lactate production. J Mol Cell Biol. 2024. https://doi.org/10.1093/jmcb/mjae021.
19. Franzen L, Olsson Lindvall M, Huhn M, Ptasinski V, Setyo L, Keith BP, et al. Mapping spatially resolved transcriptomes in human and mouse pulmonary fibrosis. Nat Genet. 2024;595:114.
20. Gul A, Yang F, Xie C, Du W, Mohammadtursun N, Wang B, et al. Pulmonary fibrosis model of mice induced by different administration methods of bleomycin. BMC Pulmon Med. 2023. https://doi.org/10.1186/s12890-023-02349-z.
21. Sun Z, Ji Z, Meng H, He W, Li B, Pan X, et al. Lactate facilitated mitochondrial fission-derived ROS to promote pulmonary fibrosis via ERK/DRP-1 signaling. J Transl Med. 2024;22(1):479.
22. Torrisi SE, Pavone M, Vancheri A, Vancheri C. When to start and when to stop antifibrotic therapies. Eur Respir Rev. 2017. https://doi.org/10.1183/16000617.0053-2017.
23. Ju X, Wang K, Wang C, Zeng C, Wang Y, Yu J. Regulation of myofibroblast dedifferentiation in pulmonary fibrosis. Respir Res. 2024;25(1):284.
24. McAnulty RJ. Fibroblasts and myofibroblasts: their source, function and role in disease. Int J Biochem Cell Biol. 2007;39(4):666–71.
25. Tang PC, Chung JY, Xue VW, Xiao J, Meng XM, Huang XR, et al. Smad3 promotes cancer-associated fibroblasts generation via macrophage-myofibroblast transition. Adv Sci. 2022;9(1):e2101235.
26. Decologne N, Kolb M, Margetts PJ, Menetrier F, Artur Y, Garrido C, et al. TGF-beta1 induces progressive pleural scarring and subpleural fibrosis. J Immunol. 2007;179(9):6043–51.
27. Loloci G, Kim YM, Choi WI, Jang HJ, Park SJ, Kwon KY. Properties of pleural mesothelial cells in idiopathic pulmonary fibrosis and cryptogenic organizing pneumonia. J Korean Med Sci. 2023;38(31):e242.
28. Kottmann RM, Trawick E, Judge JL, Wahl LA, Epa AP, Owens KM, et al. Pharmacologic inhibition of lactate production prevents myofibroblast differentiation. Am J Physiol-Lung Cel Mol Physiol. 2015;309(11):L1305–12.
29. Kang YP, Lee SB, Lee JM, Kim HM, Hong JY, Lee WJ, et al. Metabolic profiling regarding pathogenesis of idiopathic pulmonary fibrosis. J Proteome Res. 2016;15(5):1717–24.
30. Selvarajah B, Azuelos I, Anastasiou D, Chambers RC. Fibrometabolism-An emerging therapeutic frontier in pulmonary fibrosis. Sci Signal. 2021. https://doi.org/10.1126/scisignal.aay1027.
31. Wang Y, Wang X, Du C, Wang Z, Wang J, Zhou N, et al. Glycolysis and beyond in glucose metabolism: exploring pulmonary fibrosis at the metabolic crossroads. Front Endocrinol. 2024;15:1379521.
32. Cui H, Xie N, Banerjee S, Ge J, Jiang D, Dey T, et al. Lung myofibroblasts promote macrophage profibrotic activity through lactate-induced histone lactylation. Am J Respir Cell Mol Biol. 2021;64(1):115–25.
33. Saito M, Mitani A, Ishimori T, Miyashita N, Isago H, Mikami Y, et al. Active mTOR in lung epithelium promotes epithelial-mesenchymal transition and enhances lung fibrosis. Am J Respir Cell Mol Biol. 2020;62(6):699–708.
34. Saito S, Kitabatake M, Ouji-Sageshima N, Ogawa T, Oda A, Nishimura T, et al. Angiopoietin-like 4 is a critical regulator of fibroblasts during pulmonary fibrosis development. Am J Respir Cell Mol Biol. 2023;69(3):328–39.
35. Li L, Chong HC, Ng SY, Kwok KW, Teo Z, Tan EHP, et al. Angiopoietin-like 4 increases pulmonary tissue leakiness and damage during influenza pneumonia. Cell Rep. 2015;10(5):654–63.
36. Pizano-Martinez O, Mendieta-Condado E, Vázquez-Del Mercado M, Martínez-García EA, Chavarria-Avila E, Ortuño-Sahagún D, et al. Anti-drug antibodies in the biological therapy of autoimmune rheumatic diseases. J Clin Med. 2023. https://doi.org/10.3390/jcm12093271.
37. Strand V, Goncalves J, Isaacs JD. Immunogenicity of biologic agents in rheumatology. Nat Rev Rheumatol. 2021;17(2):81–97.

Publisher's Note